

# Synthesis, Structure and Characterization of a New Silicophosphate, $\text{K}_2\text{SiP}_4\text{O}_{13}$ , with a Six-fold Coordinated Si<sup>①</sup>

SUN Tong-Qing<sup>②</sup> WANG Qian-Qian

KONG Yong-Fa XU Jing-Jun

(School of Physics and the MOE Key Laboratory of Weak-light  
Nonlinear Photonics, Nankai University, Tianjin 300071, China)

**ABSTRACT** A potassium silicophosphate,  $\text{K}_2\text{SiP}_4\text{O}_{13}$ , has been synthesized in molten polyphosphoric acid. It crystallizes in the triclinic space group  $P\bar{1}$  (No. 2) with  $a = 4.8327(10)$ ,  $b = 7.7403(15)$ ,  $c = 14.485(3)$  Å,  $\alpha = 82.29(3)^\circ$ ,  $\beta = 83.31(3)^\circ$ ,  $\gamma = 81.95^\circ$ ,  $V = 529.02(19)$  Å<sup>3</sup>,  $Z = 2$ . The crystallographic structure features 2D layers of  $[\text{SiP}_4\text{O}_{13}]_\infty$  in the  $ab$  plane with counter cations  $\text{K}^+$  residing among the layers, and the anionic framework of  $[\text{SiP}_4\text{O}_{13}]_\infty$  is composed of six-fold coordinated Si atoms and tetraphosphate anions by sharing vertex O atoms. The title compound was characterized by powder X-ray diffraction, IR and Raman spectroscopies, UV-vis diffuse reflectance spectroscopy, thermogravimetry and differential scanning calorimetry.

**Keywords:** synthesis, silicophosphate,  $\text{SiO}_6$  octahedral coordination, crystal structure;

**DOI:** 10.14102/j.cnki.0254-5861.2011-2851

## 1 INTRODUCTION

Silicophosphates, also named as phosphosilicates, specially refer to the compounds with bridging P–O–Si bonds between the moieties of phosphate and silicate<sup>[1]</sup>. Non-crystalline silicophosphates have gained great industrial and academic interest for excellent chemical stability, mechanical property and photosensitivity, and can be used as optical fibers, biomaterials, luminescent materials and so on<sup>[2-4]</sup>. However, crystalline silicophosphate compounds have been developed backwardly. Though there are a large number of synthetic compounds and natural minerals in the system containing P, Si, and O elements, most of them don't belong to silicophosphates for being without P–O–Si bonds. One case is that the anionic groups of phosphorous and silicon are isolated by metal cations, and they don't share any vertex oxygen atoms to form P–O–Si bonds<sup>[5]</sup>. Another case is that phosphorous and silicon atoms disorderedly occupy the same lattice positions of crystal structure due to their close ionic radii<sup>[6, 7]</sup>. By contrast, the proportion of silicophosphates, with bridging P–O–Si bonds, are not so much in the inorganic crystalline

compounds containing P, Si and O.

As we all know, the bonding between Si and O atoms are typically four-fold coordinated. The six-fold coordination of silicon usually exists in several high pressure materials, for example,  $\text{MgSiO}_3$  ilmenite and  $\text{SiO}_2$  stishovite<sup>[8, 9]</sup>. The few oxides with  $\text{SiO}_6$  that can stably exist at ambient pressure almost have P–O–Si bonds, for instance,  $\text{SiP}_2\text{O}_7$ <sup>[10]</sup>,  $\text{Si}_5\text{O}(\text{PO}_4)_6$ <sup>[11]</sup>,  $(\text{Re}_2\text{O}_5)\text{Si}_2[\text{Si}_2\text{O}(\text{PO}_4)_6]$ <sup>[12]</sup>,  $\text{Rb}_2\text{SiP}_4\text{O}_{13}$  and  $\text{BaH}_2\text{Si}(\text{P}_2\text{O}_7)_2$ <sup>[13]</sup>. So, the field of silicophosphate is distinctive from the view point of structural chemistry.

The varieties of connection mode among  $\text{PO}_4$ ,  $\text{SiO}_4$  and  $\text{SiO}_6$  by sharing vertex oxygen atoms would give rise for structure and property variations, thus more versatile applications could be foreseeing. For example, similar to aluminosilicates, silicophosphates with different frameworks and topologies may have an important place in various scientific applications, such as molecular sieves, absorbents, and ionic conductors<sup>[1, 14]</sup>. Therefore, it is necessary to explore new silicophosphate compounds. Recently, the discoveries of  $\text{Na}_4\text{Si}_2\text{PO}_4\text{F}_9$ <sup>[15]</sup>,  $\text{K}_4\text{Si}_3\text{P}_2\text{O}_7\text{F}_{12}$  and  $\text{BaSiP}_2\text{O}_8$ <sup>[16]</sup> intensively catch the eyes of researchers for the six-fold coordinated Si

Received 16 April 2020; accepted 10 June 2020 (CCDC 1996835)

① This work was supported by the Natural Science Foundation of Tianjin City (No. 17JCYBJC17800) and the National Natural Science Foundation of China (No. 21271109 and 11674179)

② Corresponding author. E-mail: suntq@nankai.edu.cn

and P–O–Si bonds. In this paper, we reported the synthesis and structure of a new silicophosphate  $K_2SiP_4O_{13}$ , and analyzed its structural features, and characterized it by IR and Raman spectroscopies, diffuse reflectance spectroscopy and thermal analysis.

## 2 EXPERIMENTAL

### 2.1 Synthesis

Single crystals of  $K_2SiP_4O_{13}$  were synthesized by the flux method in molten polyphosphoric acid. All the reagents used in synthesis were purchased from commercial sources without further treatment.  $K_2CO_3$  (4.561 g, 33 mmol),  $SiO_2$  (0.601 g, 10 mmol) and phosphoric acid (85 wt%, 8.6 mL, 126 mmol) were mixed by stirring in a Pt crucible at room temperature. The crucible was placed in a muffle furnace oven and then heated to 400 °C in 6 h. After having been kept at 400 °C for 2 days, the temperature of the furnace was gradually decreased to 30 °C in about 10 h. The resulting products in the crucible were washed by using hot water for eliminating polyphosphoric acid and its potassium salts, and the single crystals were separated and dried in air. Eventually, colorless and narrow crystal slices of  $K_2SiP_4O_{13}$  were obtained with a yield of about 90% based on  $SiO_2$ .

### 2.2 Crystal structure determination

A single crystal of  $K_2SiP_4O_{13}$  with the size of 0.30 mm × 0.24 mm × 0.05 mm was selected for crystal structure determination. The single-crystal X-ray diffraction (XRD) data were collected on an Agilent Gemini E diffractometer with graphite-monochromated  $MoK\alpha$  radiation ( $\lambda = 0.71073$  Å) using the  $\omega$ -scan technique. The crystal was kept around 106 K during data collection. In the range of  $6.36 \leq 2\theta \leq 57.96^\circ$ , a total of 3613 reflections were collected and 2415 were independent with  $R_{int} = 0.0265$ , of which 2095 were observed with  $I > 2\sigma(I)$ . The absorption correction of multi-scan was performed. Using Olex2<sup>[17]</sup>, the structure was solved with the SHELXT<sup>[18]</sup> structure solution program using intrinsic phasing, and was refined with the SHELXL<sup>[19]</sup> refinement package using full-matrix least squares minimization on  $F^2$ . All atoms were refined with anisotropic thermal parameters. The final full-matrix least-squares refinement converged to  $R = 0.0352$ ,  $wR = 0.0814$  for the observed reflections with  $I > 2\sigma(I)$ , and  $R = 0.0419$ ,  $wR = 0.0863$  for all data. The largest diffraction peak and hole are 0.52 and  $-0.56 \text{ e} \cdot \text{\AA}^{-3}$ , respectively. The structural data were checked by the PLATON program<sup>[20]</sup>, and no higher symmetries were found. Selected bond lengths and bond angles of  $K_2SiP_4O_{13}$  are given in Table 1.

Table 1. Selected Bond Lengths (Å) and Bond Angles (°)

Bond	Dist.	Bond	Dist.	Bond	Dist.
P(1)–O(1)	1.533(2)	Si(1)–O(1) <sup>i</sup>	1.799(2)	K(1)–O(1) <sup>viii</sup>	3.457(2)
P(1)–O(2)	1.541(2)	Si(1)–O(2) <sup>ii</sup>	1.773(2)	K(2)–O(13)	2.676(2)
P(1)–O(3)	1.473(2)	Si(1)–O(5) <sup>ii</sup>	1.786(2)	K(2)–O(6)	2.701(2)
P(1)–O(4)	1.631(2)	Si(1)–O(9)	1.780(2)	K(2)–O(13) <sup>iii</sup>	2.750(2)
P(2)–O(4)	1.579(2)	Si(1)–O(11)	1.766(2)	K(2)–O(5) <sup>ix</sup>	2.827(2)
P(2)–O(5)	1.525(3)	Si(1)–O(12) <sup>iii</sup>	1.771(2)	K(2)–O(6) <sup>x</sup>	2.999(2)
P(2)–O(6)	1.460(2)	K(1)–O(8)	2.742(2)	K(2)–O(12) <sup>iii</sup>	3.151(2)
P(2)–O(7)	1.596(2)	K(1)–O(3) <sup>iv</sup>	2.794(3)	K(2)–O(11) <sup>xi</sup>	3.217(2)
P(3)–O(7)	1.593(2)	K(1)–O(8) <sup>vi</sup>	2.813(2)	K(2)–O(6) <sup>ix</sup>	3.255(3)
P(3)–O(8)	1.468(2)	K(1)–O(3) <sup>vi</sup>	2.824(2)	K(2)–O(13) <sup>ix</sup>	3.446(3)
P(3)–O(9)	1.523(2)	K(1)–O(2) <sup>i</sup>	2.922(2)	K(2)–O(4) <sup>x</sup>	3.478(2)
P(3)–O(10)	1.571(2)	K(1)–O(9) <sup>v</sup>	3.019(2)		
P(4)–O(10)	1.625(2)	K(1)–O(7) <sup>vi</sup>	3.286(2)		
P(4)–O(11)	1.541(2)	K(1)–O(1) <sup>iv</sup>	3.332(3)		
P(4)–O(12)	1.533(2)	K(1)–O(8) <sup>v</sup>	3.388(8)		
P(4)–O(13)	1.474(2)	K(1)–O(3) <sup>vii</sup>	3.451(2)		
Angle	(°)	Angle	(°)	Angle	(°)
O(1) <sup>i</sup> –Si(1)–O(2) <sup>ii</sup>	87.91(10)	O(2) <sup>ii</sup> –Si(1)–O(5) <sup>ii</sup>	93.23(9)	O(5) <sup>ii</sup> –Si(1)–O(11)	87.15(9)
O(1) <sup>i</sup> –Si(1)–O(5) <sup>ii</sup>	89.90(9)	O(2) <sup>ii</sup> –Si(1)–O(9)	86.47(9)	O(5) <sup>ii</sup> –Si(1)–O(12) <sup>iii</sup>	89.81(9)
O(1) <sup>i</sup> –Si(1)–O(9)	89.72(10)	O(2) <sup>ii</sup> –Si(1)–O(11)	179.50(10)	O(9)–Si(1)–O(11)	93.15(9)
O(1) <sup>i</sup> –Si(1)–O(11)	91.77(10)	O(2) <sup>ii</sup> –Si(1)–O(12) <sup>iii</sup>	91.56(9)	O(9)–Si(1)–O(12) <sup>iii</sup>	90.57(9)
O(1) <sup>i</sup> –Si(1)–O(12) <sup>iii</sup>	179.38(9)	O(5) <sup>ii</sup> –Si(1)–O(9)	179.52(10)	O(11)–Si(1)–O(12) <sup>iii</sup>	88.76(10)

Symmetry codes: (i)  $1 + x, y - 1, z$ ; (ii)  $x, y - 1, z$ ; (iii)  $x - 1, y, z$ ; (iv)  $1 - x, 1 - y, -z$ ; (v)  $1 + x, y, z$ ; (vi)  $2 - x, 1 - y, -z$ ;

(vii)  $1 + x, y - 1, z$ ; (viii)  $2 + x, y - 1, z$ ; (ix)  $1 - x, 1 - y, 1 - z$ ; (x)  $-x, 1 - y, 1 - z$ ; (xi)  $1 - x, -y, 1 - z$

### 2.3 Characterization of $K_2SiP_4O_{13}$

The powder XRD patterns were collected on a Bruker D8 Advance diffractometer with  $CuK\alpha$  radiation ( $\lambda = 1.5418 \text{ \AA}$ ) at room temperature in the  $2\theta$  range of  $5 \sim 70^\circ$  with a step size of  $0.02^\circ$ . The IR spectrum was recorded on a Bruker TENSOR II FTIR spectrophotometer in the range of  $400 \sim 4000 \text{ cm}^{-1}$  with KBr pressed pellet. The Raman spectrum was measured at room temperature in the range from 100 to  $3000 \text{ cm}^{-1}$ , using a Renishaw in via spectrometer under the excitation of an argon ion laser with the wavelength of 785 nm. The UV-vis diffuse reflectance spectrum was scanned in the range of  $200 \sim 800 \text{ nm}$  at room temperature on a Hitachi U-4100 spectrophotometer, with a powder pellet of  $BaSO_4$  as a standard (100% reflectance). The thermogravimetric (TG) and differential scanning (DSC) calorimetric analyses were carried out on a Setaram Setsys Evolution thermal analyzer from METTLER TOLEDO, and the samples were placed in alumina crucibles and heated at a rate of  $10^\circ\text{C}/\text{min}$  from room temperature to  $1000^\circ\text{C}$  under an atmosphere of Ar.

## 3 RESULTS AND DISCUSSION

### 3.1 Crystal structure description

$K_2SiP_4O_{13}$  crystallizes in the triclinic system,  $P\bar{1}$  (No. 2) space group with  $a = 4.8327(10)$ ,  $b = 7.7403(15)$ ,  $c = 14.485(3) \text{ \AA}$ ,  $\alpha = 82.29(3)^\circ$ ,  $\beta = 83.31(3)^\circ$ ,  $\gamma = 81.95^\circ$ ,  $V = 529.02(19) \text{ \AA}^3$  and  $Z = 2$ . Its asymmetric unit comprises of two K, one Si, four P, and thirteen O atoms, and all of them

locate on general lattice positions.  $K_2SiP_4O_{13}$  crystal features 2D layers of  $[SiP_4O_{13}]_\infty$  along the  $c$  axis, and counter cations  $K^+$  reside among the layers.

Each P atom in  $K_2SiP_4O_{13}$  is covalently bonded with four O atoms to form basic  $PO_4$  tetrahedron, and the four unique tetrahedra are linked by sharing three vertex O atoms to build a short zigzag chain, i.e. tetraphosphate anion group  $[P_4O_{13}]^{6-}$ , which is quite comparable to a fragment of a long-chain polyphosphate<sup>[21, 22]</sup>. The  $[P_4O_{13}]^{6-}$  groups are isolated from each other, and are linked by Si atoms. Each  $[P_4O_{13}]^{6-}$  interconnects with four Si atoms, and vice versa, which leads to the formation of a 2D layer of  $[SiP_4O_{13}]_\infty$  polyanion in the  $ab$  plane, as shown in Fig. 1(a). The Si atom in  $K_2SiP_4O_{13}$  is in an octahedral coordination with the O atoms from six adjacent  $PO_4$ . The six O atoms almost uniformly surround Si with nearly identical distances. The distortion index of  $SiO_6$  was calculated based on the methodology proposed by Halasyamani<sup>[23]</sup>, and its value was 0.04, which means that the  $SiO_6$  octahedron is basically undistorted. The layers of  $[SiP_4O_{13}]_\infty$  stack along the  $c$  axis, and K(1) and K(2) atoms occupy the void among the layers. Not only do they balance the electronic charges, but also join the layers by the electrostatic force between themselves and  $O^{2-}$  to build the 3D framework of  $K_2SiP_4O_{13}$ , as shown in Fig. 1(b). The coordination environments around the K atoms are rather irregular, and the K–O distances vary in a rather wide range of  $2.676(2) \sim 3.478(2) \text{ \AA}$ .

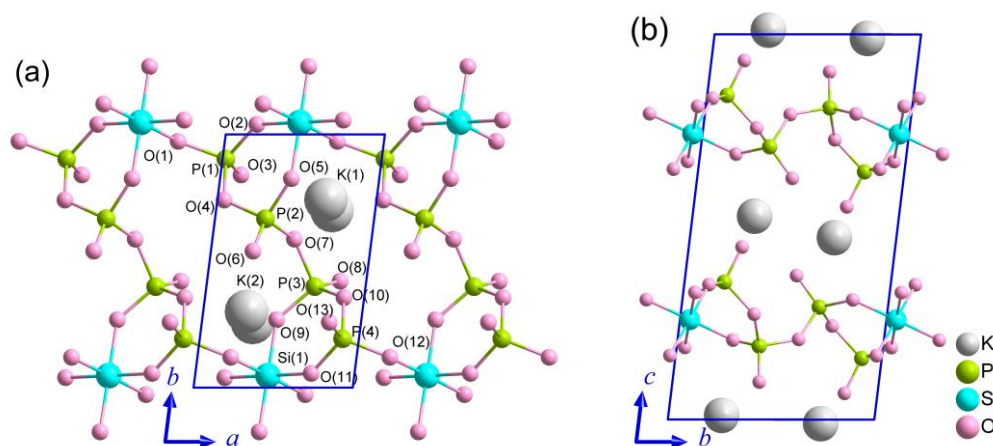


Fig. 1. (a) View of the  $[SiP_4O_{13}]_\infty$  layer in the  $ab$  plane and the  $K^+$  ions in the cavities, (b) Projection of the  $K_2SiP_4O_{13}$  crystallographic structure along the  $a$  axis

The bond valences (BV)<sup>[24]</sup> and bond valence sums (BVS) of all atoms in  $K_2SiP_4O_{13}$  were calculated, with the results listed in Table 2. The calculated BVS value of each atom is in good agreement with its corresponding oxidation number. It

should be noted that thirteen independent O atoms can be divided into three groups according to their bonding characters. The first group consists of the bridge oxygen atoms of P–O–P, i.e., O(4), O(7) and O(10), which have the

longest bond lengths of P–O in each PO<sub>4</sub> tetrahedron. The second one includes the bridging O atoms bonding with P and Si: O(1), O(2), O(5), O(9), O(11), and O(12). Finally, the terminal oxygen atoms of PO<sub>4</sub> tetrahedra, i.e. O(3), O(6), O(8) and O(13), belong to the third group, which has the shortest distances of P–O and correspondingly, the highest BV values

in each tetrahedron. The average values of BVS for these three groups are 2.13, 2.03, and 1.88, respectively, which reflects well the differences of O atoms on the bonding environments in K<sub>2</sub>SiP<sub>4</sub>O<sub>13</sub> that brings rich stretching vibrations in the IR and Raman spectra.

Table 2. Bond Valences (BV) and Bond Valence Sums (BVS) in K<sub>2</sub>SiP<sub>4</sub>O<sub>13</sub>

BV	P(1)	P(2)	P(3)	P(4)	Si(1)	K(1)	K(2)	BVS
O(4)	0.964	1.110					0.026	2.10
O(7)		1.059	1.067			0.044		2.17
O(10)			1.133	0.979				2.11
O(1)	1.253				0.651	0.039 0.028		1.97
O(2)	1.227				0.699	0.118		2.04
O(5)		1.282			0.673		0.153	2.11
O(9)			1.289		0.685	0.091		2.06
O(11)				1.228	0.711		0.053	1.99
O(12)				1.255	0.702		0.064	2.02
O(3)	1.476					0.167 0.154 0.028		1.83
O(6)		1.528					0.215 0.096 0.048	1.89
O(8)			1.494			0.192 0.159 0.034		1.88
O(13)				1.471			0.230 0.188 0.029	1.92
BVS	4.92	4.98	4.98	4.93	4.12	1.05	1.10	

K<sub>2</sub>SiP<sub>4</sub>O<sub>13</sub> crystal is isostructural with its homologue, Rb<sub>2</sub>SiP<sub>4</sub>O<sub>13</sub><sup>[13]</sup>, of which cell parameters are  $a = 4.8327(10)$ ,  $b = 7.7403(15)$  and  $c = 14.485(3)$  Å. In comparison to those of Rb<sub>2</sub>SiP<sub>4</sub>O<sub>13</sub>, the dimensions of  $a$  and  $b$  axes of K<sub>2</sub>SiP<sub>4</sub>O<sub>13</sub> don't generate obvious changes (less than 0.5%) though the ion radius of K<sup>+</sup> (1.51 Å) is obviously smaller than that of Rb<sup>+</sup> (1.61 Å). Meanwhile, the dimension of the  $c$  axis decreases 4%, which implies that the 2D network of [SiP<sub>4</sub>O<sub>13</sub>]<sub>∞</sub> is rigid parallel to the  $ab$  plane and the size of the cavities along the  $c$  axis occupied by the alkali metal cations is delimited by it. When Na<sup>+</sup> with smaller size (1.18 Å) residing the cavities, the long distances of Na–O would make the structure instable. On the contrary, the cavities could not accommodate bigger cation, such as Cs<sup>+</sup> (1.74 Å). It may be the reason that the isostructural silicophosphates of Na<sup>+</sup> and Cs<sup>+</sup> have not been

successfully synthesized. With the substitution of Si<sup>4+</sup> (0.40 Å) by Ge<sup>4+</sup> (0.53 Å) or Ti<sup>4+</sup> (0.61 Å), the sizes of the cavities would increase and could hold bigger alkali metal cation. Therefore, Cs<sub>2</sub>GeP<sub>4</sub>O<sub>13</sub><sup>[25]</sup> and Cs<sub>2</sub>TiP<sub>4</sub>O<sub>13</sub><sup>[26]</sup> that are isostructural with K<sub>2</sub>SiP<sub>4</sub>O<sub>13</sub> and Rb<sub>2</sub>SiP<sub>4</sub>O<sub>13</sub> can stably exist.

The sample for powder XRD was prepared by pulverizing and grinding the synthesized crystals, and Fig. 2 presents the experimental XRD pattern accompanied with the simulated one by Powder Cell<sup>[27]</sup> based on the single-crystal structure. The positions of diffraction peaks between them are completely identical with each other, and so do the intensities basically except for the multiple diffraction of (001), whose experimental peaks are greatly stronger than the simulated ones. This shows a strong preferred orientation in the tested powder XRD sample. The [SiP<sub>4</sub>O<sub>13</sub>]<sub>∞</sub> layer is fully composed

of strong covalent interactions of Si–O and P–O in the *ab* plane. By contrast, the layers are interconnected along the *c* axis only by weak electrostatic forces between  $K^+$  and  $O^{2-}$ . So,

$K_2SiP_4O_{13}$  is very apt to cleavage parallel to the (001) crystal face. The slice-like crystallization habit of  $K_2SiP_4O_{13}$  is also related to its special layered structure.

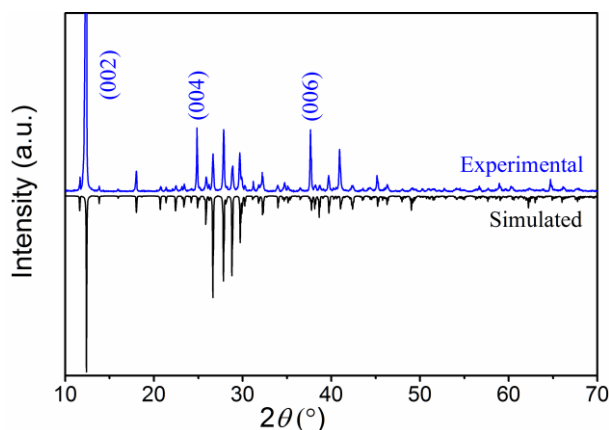


Fig. 2. Experimental XRD pattern of the pulverized  $K_2SiP_4O_{13}$  crystals

### 3.2 IR and Raman spectra

IR and Raman spectra of  $K_2SiP_4O_{13}$  are presented in Fig. 3. On the basis of literature reports<sup>[3, 4, 7, 28-32]</sup>, the stretching vibrations in the IR spectrum could be divided mainly to four regions. The broad band in region I is attributed to the O–P–O stretching vibrations of the terminal oxygen atoms, which are sometimes called as doubly bonded oxygen vibrations. The intensive band around  $1060\text{ cm}^{-1}$  in region II is assigned to the O–P–O stretching vibrations of the bridging oxygen atoms

in  $PO_4$  tetrahedra while the band around  $940\text{ cm}^{-1}$  (region III) to the O–Si–O stretching vibrations in the  $SiO_6$  octahedron. The bands in region IV are attributed to the stretching vibrations of P–O–P and P–O–Si. The assignments of the stretching vibrations in the Raman spectrum are principally identical with those in the IR spectrum. The bands below  $600\text{ cm}^{-1}$  are attributed to the bending vibrations of  $PO_4$  and  $SiO_6$  structural units and the harmonics of stretching vibrations.

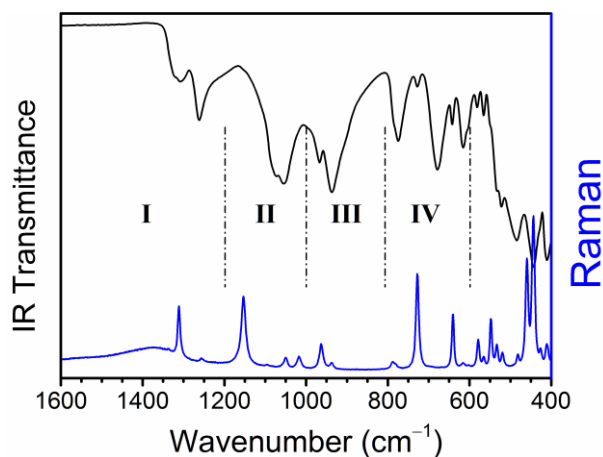


Fig. 3. IR and Raman spectra of  $K_2SiP_4O_{13}$

### 3.3 UV-vis diffuse reflectance spectrum

Fig. 4 shows the UV-vis diffuse reflectance spectrum of  $K_2SiP_4O_{13}$ . The absorption spectrum was calculated from the diffuse reflectance spectrum using the Kubelka-Munk function:  $F(R) = (1 - R)^2/2R = K/S$ , where  $R$  represents the reflectance,  $K$  the absorption, and  $S$  the scattering. In a  $F(R)$  versus  $E(\text{eV})$  plot, extrapolating the linear part of the rising

curve to zero provides the onset of absorption. Based on the inset of Fig. 4, the optical band gap of  $K_2SiP_4O_{13}$  is estimated to be 4.85 eV, which is much wider than that of  $Cs_2GeP_4O_{13}$  (4.07 eV)<sup>[25]</sup>. However, the band gap of  $K_2SiP_4O_{13}$  is narrow by contrast with the phosphates of alkali metals or alkali earth metals<sup>[33, 34]</sup>, which should be related to the electronic transition of the Si–O bonds<sup>[35]</sup>.

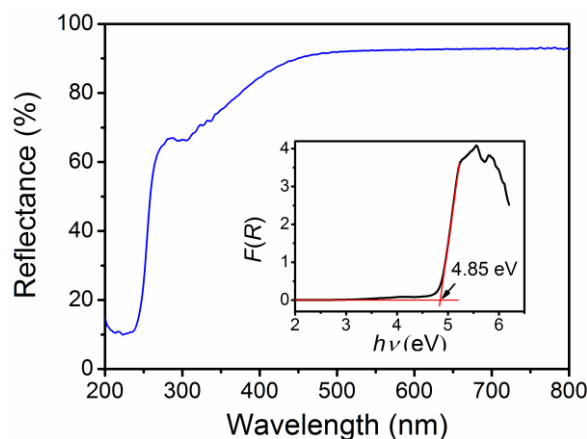


Fig. 4. UV-vis diffuse reflectance spectrum of  $\text{K}_2\text{SiP}_4\text{O}_{13}$

### 3.4 Thermal properties

Fig. 5 presents the TG-DSC curves of  $\text{K}_2\text{SiP}_4\text{O}_{13}$ . A sharp endothermic peak was observed at 730 °C while the sample weight didn't show a representative change in the whole temperature range. The isostructural compound  $\text{Rb}_2\text{SiP}_4\text{O}_{13}$  was reported to decompose at 723 °C, however, no more information was mentioned<sup>[13]</sup>. In order to clarify whether the title compound melts or decomposes at high temperature, a sample of pulverized  $\text{K}_2\text{SiP}_4\text{O}_{13}$  crystal was heated at 800 °C for two hours, and then the sample was very quickly decreased to room temperature. White solidified polycrystalline substances mixed glassy things were observed. The sample after heat-treating was analyzed by powder XRD. As

shown in the inset of Fig. 5,  $\text{K}_2\text{SiP}_4\text{O}_{13}$  should decompose in accordance with the reaction:  $\text{K}_2\text{SiP}_4\text{O}_{13} \rightarrow \text{Si}_5\text{O}(\text{PO}_4)_6 + \text{amorphous phase}$ . The amorphous phase probably contained phosphorus and potassium oxides since the sample weight remained roughly constant. The approximate decomposition temperature of  $\text{K}_2\text{SiP}_4\text{O}_{13}$  and  $\text{Rb}_2\text{SiP}_4\text{O}_{13}$  indicates that the rigid 2D network of  $[\text{SiP}_4\text{O}_{13}]_\infty$  could play a crucial role in their thermal stability. After comparing with the structure of  $\text{Si}_5\text{O}(\text{PO}_4)_6$ <sup>[11]</sup>, it should be mentioned that the majority of Si atoms originally in  $\text{K}_2\text{SiP}_4\text{O}_{13}$  still kept an octahedron coordination after heat decomposition while the short zigzag chain of  $[\text{P}_4\text{O}_{13}]^{6-}$  was broken.

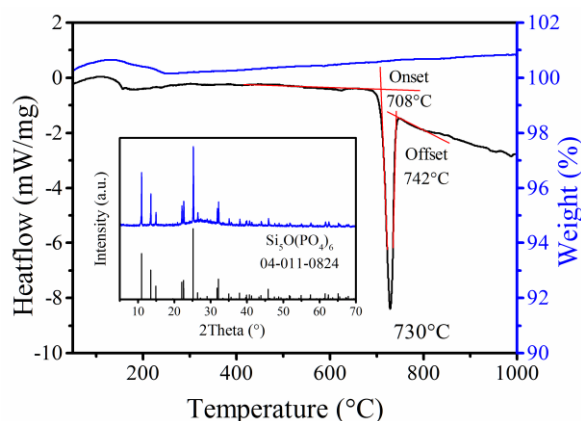


Fig. 5. TG and DSC curves of the  $\text{K}_2\text{SiP}_4\text{O}_{13}$  pulverized crystals and the powder XRD pattern of their thermal decomposition products (inset)

## 4 CONCLUSION

In summary, we have synthesized a new silicophosphate compound,  $\text{K}_2\text{SiP}_4\text{O}_{13}$ , by the flux method. The crystallographic structure features a 2D network of  $[\text{SiP}_4\text{O}_{13}]_\infty$  stacking along the *c* axis, which is composed of tetraphosphate anions

interconnected by Si atoms in a hardly distorted octahedral coordination. The IR and Raman vibration spectra reflect the structural characteristics of  $\text{K}_2\text{SiP}_4\text{O}_{13}$ . The compound is thermally stable up to 730 °C, and then decomposes to  $\text{Si}_5\text{O}(\text{PO}_4)_6$ . Its optical band gap was estimated to be about 4.85 eV by diffuse reflectance spectroscopy.

## REFERENCES

- (1) Styskalik, A.; Babiak, M.; Machac, P.; Relichova, B.; Pinkas, J. New adamantane-like silicophosphate cage and its reactivity toward tris(pentafluorophenyl)borane. *Inorg. Chem.* **2017**, 56, 10699–10705.
- (2) Zeng, H. D.; Jiang, Q.; Liu, Z.; Li, X.; Ren, J.; Chen, G. R.; Liu, F. D.; Peng, S. Unique sodium phosphosilicate glasses designed through extended topological constraint theory. *J. Phys. Chem. B* **2014**, 118, 5177–5193.
- (3) Sawangboon, N.; Nizamutdinova, A.; Uesbeck, T.; Limbach, R.; Meechoowas, E.; Tapasa, K.; Möncke, D.; Wondraczek, L.; Kamitsos, E. I.; Wüllen, L. V.; Brauer, D. S. Modification of silicophosphate glass composition, structure, and properties via crucible material and melting conditions. *Int. J. Appl. Glass Sci.* **2020**, 11, 46–57.
- (4) Abdelghany, A. M.; Zeyada, H. M.; ElBatal, H. A.; Fetouh, R. Synthesis and spectral properties of  $Nd_2O_3$ -doped sodium silicophosphate glass. *Silicon* **2016**, 8, 325–330.
- (5) Unithrattil, S.; Arunkumar, P.; Kim, Y. H.; Kim, H. J.; Vu, N. H.; Heo, J.; Chung, W. J.; Im, W. B. A phosphosilicate compound,  $NaCa_3PSiO_8$  structure solution and luminescence properties. *Inorg. Chem.* **2017**, 56, 15130–15137.
- (6) Deng, Y.; Eames, C.; Chotard, J. N.; Lalère, F.; Seznec, V.; Emge, S.; Pecher, O.; Grey, C. P.; Masquelier, C.; Islam, M. S. Structural and mechanistic insights into fast lithium-ion conduction in  $Li_4SiO_4$ - $Li_3PO_4$  solid electrolytes. *J. Am. Chem. Soc.* **2015**, 137, 9136–9145.
- (7) Porkodi, P.; Yegnaraman, V.; Kamaraj, P.; Kalyanavalli, V.; Jeyakumar, D. Synthesis of NASICON — a molecular precursor-based approach. *Chem. Mater.* **2008**, 20, 6410–6419.
- (8) Stearns, L. A.; Groy, T. L.; Leinenweber, K. High-pressure synthesis and crystal structure of silicon phosphate hydroxide,  $SiPO_4(OH)$ . *J. Solid State Chem.* **2005**, 178, 2594–2061.
- (9) Kowalke, J.; Arnold, C.; Ponomarev, I.; Jäger, C.; Kroll, P.; Brendler, E.; Kroke, E. Structural insight into layered silicon hydrogen phosphates containing  $[SiO_6]$  octahedra prepared by different reaction routes. *Eur. J. Inorg. Chem.* **2019**, 828–836.
- (10) Leinenweber, K.; Stearns, L. A.; Nite, J. M.; Németh, P.; Groy, T. L. Structure of a new form of silicon phosphate ( $SiP_2O_7$ ) synthesized at high pressures and temperatures. *J. Solid State Chem.* **2012**, 190, 221–225.
- (11) Poojary, D. M.; Borade, R. B.; Clearfield, A. Structural characterization of silicon orthophosphate. *Inorg. Chim. Acta* **1993**, 208, 23–29.
- (12) Islam, S. M.; Glaum, R.; Pelka, A.; Daniels, J.; Hoffbauer, W. The first phosphates of heptavalent rhenium. *Z. Anorg. Allg. Chem.* **2013**, 639, 2463–2472.
- (13) Koenigstein, K.; Jansen, M. Ein einfacher weg zu silicium in oktaedrischer sauerstoffkoordination. *Chem. Ber.* **1994**, 127, 1213–1218.
- (14) Khabbouchia, M.; Hosnia, K.; Meznia, M.; Srasraa, E. Simplified synthesis of silicophosphate materials using an activated metakaolin as a natural source of active silica. *Appl. Clay Sci.* **2018**, 158, 169–176.
- (15) Ding, Q. R.; Zhao, S. E.; Xiao, H.; Li, Y. Q.; Liu, S.; Li, L. N.; Li, C. S.; Wang, Y. S.; Hong, M. C.; Luo, J. H. An uncommon hypervalent fluorooxosilicophosphate. *Chem. Asian J.* **2019**, 14, 4174–4178.
- (16) Han, G. P.; Lei, B. H.; Yang, Z. H.; Wang, Y.; Pan, S. L. A fluorooxosilicophosphate with an unprecedented  $SiO_2F_4$  species. *Angew. Chem. Int. Ed.* **2018**, 57, 9828–9832.
- (17) Dolomanov, O. V.; Bourhis, L. J.; Gildea, R. J.; Howard, J. A. K.; Puschmann, H. OLEX2: a complete structure solution, refinement and analysis program. *J. Appl. Cryst.* **2009**, 42, 339–341.
- (18) Sheldrick, G. M. SHELXT – integrated space-group and crystal-structure determination. *Acta Cryst.* **2015**, A71, 3–8.
- (19) Sheldrick, G. M. Crystal structure refinement with SHELXL. *Acta Cryst.* **2015**, C71, 3–8.
- (20) Spek, A. L. Structure validation in chemical crystallography. *Acta Cryst.* **2009**, D65, 148–155.
- (21) Zhao, S. E.; Gong, P. F.; Luo, S. Y.; Bai, L.; Lin, Z. S.; Ji, C. M.; Chen, T. L.; Hong, M. C.; Luo, J. H. Deep-ultraviolet transparent phosphates  $RbBa_2(PO_3)_5$  and  $Rb_2Ba_3(P_2O_7)_2$  show nonlinear optical activity from condensation of  $[PO_4]^{3-}$  units. *J. Am. Chem. Soc.* **2014**, 136, 8560–8563.
- (22) Zhong, Y.; Shan, P.; Sun, T. Q.; Hu, Z. P.; Liu, H. D.; Liu, S. G.; Kong, Y. F.; Xu, J. J. Growth and theoretical study on the deep ultraviolet transparent  $\beta$ - $CsBa_2(PO_3)_5$  nonlinear optical crystal. *CrystEngComm.* **2019**, 21, 4690–4695.
- (23) Halasyamani, P. S. Asymmetric cation coordination in oxide materials: influence of lone-pair cations on the intra-octahedral distortion in  $d^0$  transition metals. *Chem. Mater.* **2004**, 16, 3586–3592.
- (24) Brown, I. D. Recent developments in the methods and applications of the bond valence model. *Chem. Rev.* **2009**, 109, 6858–6919.
- (25) Zhao, D.; Xie, Z.; Hu, J. M.; Zhang, H.; Zhang, W. L.; Yang, S. L.; Cheng, W. D. Structure determination, electronic and optical properties of  $NaGe_2P_3O_{12}$  and  $Cs_2GeP_4O_{13}$ . *J. Mol. Struct.* **2009**, 922, 127–134.

- (26) Chudinova, N.; Murashova, E. Synthesis and structure of double phosphates of titanium and alkalimetals. *Proc. Est. Acad. Sci. Chem.* **2000**, 49, 29–35.
- (27) Kraus, W.; Nolze, G. POWDER CELL — a program for the representation and manipulation of crystal structures and calculation of the resulting X-ray powder patterns. *J. Appl. Cryst.* **1996**, 29, 301–303.
- (28) Schildhammer, D.; Fuhrmann, G.; Petschnig, L. L.; Wurst, K.; Vitzthum, D.; Seibald, M.; Schottenberger, H.; Huppertz, H. Structural redetermination and photoluminescence properties of the niobium oxyphosphate  $(\text{NbO})_2\text{P}_4\text{O}_{13}$ . *Inorg. Chem.* **2017**, 56, 2736–2741.
- (29) Rao, K. J.; Baskaran, N.; Ramakrishnan, P. A.; Ravi, B. G.; Karthikeyan, A. Structural and lithium ion transport studies in sol gel-prepared lithium silicophosphate glasses. *Chem. Mater.* **1998**, 10, 3109–3123.
- (30) Calahoo, C.; Zwanziger, J. W.; Butler, I. S. Mechanical-structural investigation of ion-exchanged lithium silicate glass using micro-Raman spectroscopy. *J. Phys. Chem. C* **2016**, 120, 7213–7232.
- (31) Arroyabe, E.; Kaindl, R.; Többs, D. M.; Kahlenberg, V. Synthesis, crystal structure, and vibrational spectroscopy of  $\text{K}_2\text{Ca}_4\text{Si}_8\text{O}_{21}$  — an unusual single-layer silicate containing  $\text{Q}^2$  and  $\text{Q}^3$  units. *Inorg. Chem.* **2009**, 48, 11929–11934.
- (32) Zhu, Z. Y.; Gu, S. X.; Li, S. S.; Chen, C.; Xiao, S. Q.; Tao, H. Z. Effects of six-fold coordinated silicon on structure and properties of  $\text{BaO-SiO}_2\text{-P}_2\text{O}_5$  glasses. *J. Wuhan Univ. Technol.-Mat. Sci. Ed.* **2019**, 34, 1043–1048.
- (33) Bai, Z. Y.; Hu, C. L.; Liu, L. H.; Zhang, L. Z.; Huang, Y. S.; Yuan, F. F.; Lin, Z. B.  $\text{KMg}(\text{H}_2\text{O})\text{PO}_4$ : a deep-ultraviolet transparent nonlinear optical material derived from  $\text{KTiOPO}_4$ . *Chem. Mater.* **2019**, 31, 9540–9545.
- (34) Bai, Z. Y.; Liu, L. H.; Zhang, L. Z.; Huang, Y. S.; Yuan, F. F.; Lin, Z. B.  $\text{K}_2\text{SrP}_4\text{O}_{12}$ : a deep-UV transparent cyclophosphate as a nonlinear optical crystal. *Chem. Commun.* **2019**, 55, 8454–8457.
- (35) Lee, M. H.; Yang, C. H.; Jan, J. H. Band-resolved analysis of nonlinear optical properties of crystalline and molecular materials. *Phys. Rev. B* **2004**, 70, 235110.